Experimental Investigation of a Large-Diameter Cathode

Matthew L. Plasek,* Christopher J. Wordingham,* Sebastián Rojas Mata,*

Nicolas Luzarraga,† Edgar Y. Choueiri‡

Electric Propulsion and Plasma Dynamics Laboratory

Princeton University, Princeton, NJ 08544 USA

James E. Polk§

Jet Propulsion Laboratory, California Institute of Technology, M/S 125-109

4800 Oak Grove Drive, Pasadena, CA 91109 USA

A large-diameter lanthanum hexaboride hollow cathode has been experimentally investigated at discharge currents of 20 to 225 A as part of the development of the RF-Controlled Hollow Cathode. Hollow cathodes used in the next generation of Hall thrusters will have to produce 300 to 700 A of discharge current while operating for tens of thousands of hours. This large-diameter cathode is a proof-of-concept experiment intended to address both long-life and high-current operation. Cathode current-voltage characteristics and temperature profiles were measured with varied discharge currents, mass flow rates, and gas species. Using krypton allowed for plasma ignition at lower voltages than argon for comparable flow rates, and current-voltage characteristics measured with krypton qualitatively match cathode behavior in the literature. While operating at 20 A, cathode temperatures decreased for both argon and krypton with increasing mass flow, contrasting with prior large-cathode behavior. Finally, heater-insulating boron nitride was found to chemically interact with tungsten wire heaters at high temperatures causing frequent heater failures; graphite standoffs are a proposed solution.

I. Introduction

Recent trends in hollow cathode research reflect the needs of proposed missions and projected capabilities at much higher current levels than the current state of the art. The U.S. Air Force Research Laboratory (AFRL) projects that electric thrusters will need to process 100-200 kW of power "for near- to mid-term propulsion capabilities."[1] At the moderate specific impulses of AFRL interest (between 2000-6000 seconds), this translates to roughly 330-660 A of discharge current. NASA also continues to show interest in higher thruster powers; hall thrusters are being developed in the 20-100 kW power range which can require discharge currents up to 400 A.[2] For example, a 50 kW-class Hall thruster has been developed at NASA and was tested up to 100 A of discharge current as reported in 2012.[3] In addition to cathodes capable of providing discharge currents from 300-700 A, proposed missions would also require lifetimes longer than 10 kh.[2] As seen in previously proposed nuclear electric propulsion missions, lifetimes for interplanetary missions could approach as much as 100 kh.[4] 100-200 kW power requirements for thrusters exemplify the need for new hollow cathodes that are explicitly designed to handle high discharge currents while providing extended operational life.

Progress towards high-current, long-lifetime hollow cathodes has been made by Goebel and Chu[5,6] in testing a lanathanum hexaboride (LaB_6) bulk-emitting hollow cathode at up to 300 A of discharge current

*Graduate Research Assistant, EPPDyL; Mechanical and Aerospace Engineering Dept., Student Member AIAA.

†Undergraduate Research Assistant, EPPDyL; Mechanical and Aerospace Engineering Dept.

‡Chief Scientist, EPPDyL; Professor, Applied Physics Group, Mechanical and Aerospace Engineering Dept.; Fellow AIAA.

§Principal Engineer, Propulsion and Materials Engineering Section, Associate Fellow AIAA

while maintaining an expected life of 10-20 kh. Van Noord, et al.[7] describe the design and testing of a dispenser cathode at 50 A with a predicted life of 100 kh. Even with these selected advances, the expected improvement needed over the next few decades demands novel cathode concepts that can feasibly approach *both* lifetimes up to 100 kh and discharge currents up to 700 A.

The RF-Controlled Hollow Cathode is a proof-of-concept experiment that attempts to address these requirements by adding radio-frequency (RF) power to a thermionic hollow cathode. The difference between the RF-Controlled Hollow Cathode and other RF cathodes in the literature[8,9] is that we are adding RF power to a high-current LaB_6 thermionic hollow cathode. Combining the thermionic hollow cathode and RF cathode concepts allows for a high current source with significant potential for performance enhancement from the added RF power. The basic principle behind the expected benefit to hollow cathode performance is that the added RF power will alter the plasma density and emitter temperature profiles along the length of the cathode major axis.

For state-of-the-art hollow cathodes in use today a sharp peak in the axial profile of the plasma density within the internal cavity corresponds to a small current "attachment," or plasma-emitter contact, area. This restricted current attachment area leads to high current densities and high temperatures within a limited axial depth inside the cathode.[10–12] Upstream of this dense-plasma region, the plasma density is not high enough to support significant thermionic emission and so the emission is space-charge limited,[13] as shown schematically in Fig. 1. Emitting significant electron emission from the full axial length of the emitter (e.g. 20 A/cm^2 for LaB_6)[14] requires that the profiles of both the plasma density and emitter temperature be "flatter" and uniformly greater than minimum values (for the above example, about 2×10^{19} m^{-3} and 1700°C)[15] along the axial length of the emitter. When relatively uniform profiles are not possible, undesirable peaks in these axial profiles create regions that emit at higher temperatures and current densities, reducing the life of the emitter due to evaporation, while the remaining regions lack significant current density due to space-charge-limiting effects.[13]

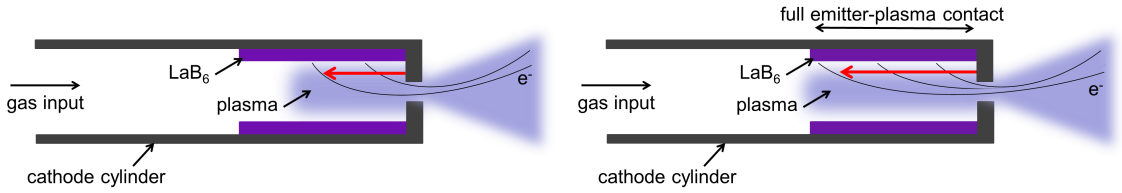

Figure 1. Cutaway side views of a basic hollow cathode showing the typical limited current attachment area along the length of the LaB_6 emitter (left) compared to the goal of current attachment to the full emitter area (right).

Approaching the desired flat, uniform profiles of emitter temperature and internal plasma density allows the operator to choose some optimal balance between increasing the operational lifetime and increasing the discharge current to desired levels. This is the goal of adding RF power to a thermionic hollow cathode: to control or alter the axial profiles of plasma density and emitter temperature such that there is significant current attachment along the entire length of the emitter.

We previously simulated[15,16] the effects of RF power input in one configuration of the RF-Controlled Hollow Cathode with a simplified two-dimensional numerical model. This model suggested that added RF power would significantly increase the plasma density in the upstream portion of the emitter region, enhancing thermionic emission from more of the emitter area. These results supported further experimental investigation of the RF-Controlled Hollow Cathode.

We have designed and constructed an RF-Controlled Hollow Cathode experiment and testing is ongoing. We refer to this experiment as the RFC Cathode herein, although this is not to be confused with low-current hollow cathodes that do not have a low-work-function thermionic insert but also have RF input. In this paper we address the design and operational challenges of high-temperature heaters, critical elements of thermionic hollow cathodes, as well as the ignition and operational characteristics of large-scale hollow cathodes.

Starting in Section II we describe the novel elements and overall design of the RFC Cathode. Then, in Section III, we describe our experimental setup. Finally, our results are presented in Section IV with a characterization of a large-diameter cathode, and a discussion of insights that address some of the new challenges presented by large-scale hollow cathodes and high-temperature heaters.

II. Design Features of Large-Diameter RFC Cathode

The large inner diameter of the RFC Cathode was driven by the need for the insert diameter to contain the circular-waveguide cutoff-wavelength of the selected 8 GHz microwave input frequency. The selection of an 8 GHz microwave frequency in the RF spectrum was derived from a trade-off study between the cathode inner diameter (acting as a waveguide), attainable RF plasma densities, RF coupling methods, and the cost and availability of an RF generator and amplifier. The resulting inner diameter of the RFC Cathode is 2.7 cm, which is approximately twice the inner diameter of any other LaB_6 hollow cathode developed to date. In addition to allowing RF input, the size of the RFC Cathode presents a unique opportunity to study the behavior of large-scale thermionic hollow cathodes.

We have previously explained the selection of an 8 GHz input frequency, the design of this RFC Cathode configuration, and have given a summary of the behavior of large-diameter hollow cathodes from the literature in Ref. 15. In general, both a larger cathode diameter[7,17–19] and added RF power[16] are expected to increase the maximum discharge current while lowering current densities. Next, we detail specific elements of the design which impact the operation of a large-diameter bulk-emitting hollow cathode.

A. Cathode Assembly

Figure 2 shows to-scale side-cutaway views of our RFC Cathode design. The press-sintered LaB_6 that comprises the emitter region, where the insert plasma is generated, is shown in purple. Depicted by the orange arrows in the right image in Figure 2, microwaves travel into the cathode tube (which is effectively a waveguide) and through a white disk made of hexagonal boron nitride. The disk serves both as a low-loss microwave window and a gas barrier in the cathode waveguide tube. We chose an axial disk thickness to be half of the incident wavelength (1.0 cm thick at 8 GHz) in order to maximize the transmittance.

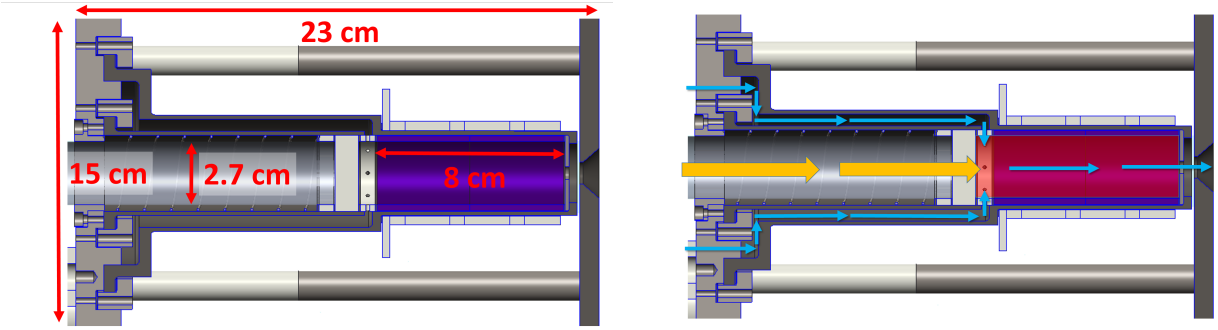

Figure 2. Side cutaway views of the RFC Cathode created in CAD software. The purple region in the left image is the LaB_6 emitter tube insert. In the right image, the orange arrows depict microwave propagation in waveguide, light blue arrows depict the neutral gas injection path, and the red overlay is the emitter region and internal cavity. Plasma exits downstream through the orifice to the right. The heater and heater radiation shielding are not pictured.

Neutral gas is injected through the gray stainless steel base into an annular region between the two dark-gray graphite cylinders, where it travels downstream and then moves radially inward into the emitter region immediately after the microwave window. A two-dimensional view of this path is depicted by the light blue arrows in Figure 2. This novel gas injection scheme was used to prevent gas leakage into the waveguide portion of the cathode (potentially creating an unwanted plasma in the upstream waveguide) and to remove the need for costly and potentially problematic high-temperature brazes or welds on the downstream portion of the cathode.

We chose lanthanum hexaboride as an insert material due to its significantly higher poisoning resistance than typical dispenser cathode emitters, which allows for simplified handling and startup procedures.[14] LaB_6 as an emitter material also shows longer simulated lifetimes than dispenser cathode emitters,[2,14] the ability to emit current densities above 20 A/cm^2,[14] and has demonstrated discharge currents up to 300 A.[13] In the RFC Cathode design, we chose the long emitter insert length (8 cm), significantly longer than seen in other large hollow cathode experiments (e.g. 5 cm),[20] so that we can more easily measure and discern the effect of RF input power on the axial profiles of plasma density and emitter temperature.

The RFC Cathode is significantly larger than previous large-cathode experiments and, as the cathode is a proof-of-concept, experimental lab article only, we limited the keeper to a graphite disk suspended between the cathode and anode. By not entirely enclosing the cathode in a graphite keeper, we gained access to the outside tube surface of the emitter region to place thermocouples and heater leads. This results in the RFC Cathode suffering greater radiative losses due to less complete shielding. However, most of the radiation is reflected by three slotted molybdenum heat shields that are separated from one another to prevent thermal conduction. We electrically isolated the heat shields from one another to eliminate one significant source of arcing during operation, which was exacerbated by the sharp edges of the foil shields.

B. Heater

The heater is a critical element of a thermionic hollow cathode.[21] The heater is used to preheat the cathode's emitter material to a temperature at which significant thermionic emission can take place and a cathode plasma can be ignited. For a large-diameter hollow cathode, losses increase substantially with the radius and the power input required to get to nominal operating temperatures is significant. For comparison, the typical heater power required to reach a peak axial temperature of 1450°C on the RFC Cathode is around 4 kW, versus 0.4 kW for the largest cathode reported by Goebel and Chu.[5] We expect that the heater input power could be lowered with better shielding, although retaining access to the cathode for measurements makes further shielding difficult. This power requirement could also be reduced by improving the thermal contact between the heater and cathode tube.

Due to the relatively high radiative thermal losses derived from the scale and shielding of the RFC Cathode as well as unoptimized thermal contact between the heater and cathode, depositing high power results in heater temperatures exceeding 1800°C. This precludes the use of many high-temperature materials for heater insulation that are electrically insulating but retain significant thermal conductivity at these temperatures. We have used a bare tungsten wire as a resistive heater, but we have experienced problems including arcing, stable but undesirable current attachment to the heater, embrittlement due to recrystallization, and undesirable chemical reactions with insulators at high temperatures. Specific electrical and physical heater details can be found in Section III with the results and operational description of our evolving heater design in Section IV.

III. Experimental Apparatus

A. Vacuum Facility

The RF-Controlled Hollow Cathode experiment was fabricated and tested in the Electric Propulsion and Plasma Dynamics Laboratory (EPPDyL) at Princeton University. A fiberglass tank, 2 m in diameter and 5 m in length, was evacuated to the 6×10^{-5} Torr range by two 0.0708 m^3/s mechanical roughing pumps, a 0.632 m^3/s roots blower and two 95 m^3/s diffusion pumps. During cathode operation, the background pressure stayed in the high 10^{-5} to low 10^{-4} Torr range, and during measurements did not exceed 3×10^{-4} Torr, as measured by ionization gauges.

B. Cathode Configuration

An enlarged view of the emitter region of the cathode assembly is presented in Figure 3. The cathode components were all housed inside an 8.45 cm long graphite tube (grade AXM-5Q from Entegris/Poco Graphite). A lip on the downstream end of the tube held a tungsten orifice plate with a 0.56 cm diameter orifice. To prevent boron diffusion, a graphite foil "washer" (grade GTB Grafoil) separated this tungsten plate from the thermionically emitting lanthanum hexaboride inserts (99.5% pure from Materion). These inserts consisted of two 4 cm long, 2.7 cm inner diameter, 3.2 cm outer diameter tubes in contact with each other. Upstream of the inserts, we placed a boron nitride ring (grade AX05 from Saint Gobain) in contact with the LaB_6. Six evenly-spaced radial holes were drilled into the boron nitride ring for gas input. Further upstream we placed a 1 cm thick boron nitride disk (acting as a microwave window and gas break) and a second boron nitride ring to distribute pressure along the disk's edge, all separated with more graphite foil "washers." The flexible graphite foil was cut into washer shapes that can compress and recoil. These properties allowed us to use the graphite foil as a seal to prevent gas flow upstream of the microwave window (or gas break). A tungsten spring upstream of the boron nitride pieces provided a force to keep all interior

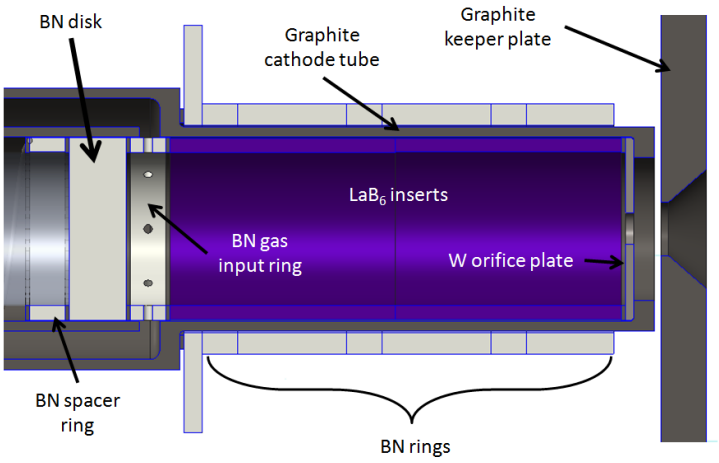

Figure 3. A side cutaway view of emitter region of the RFC Cathode.

cathode components in place and in contact. Surrounding the outside of the graphite tube were six boron nitride insulating rings, three of which had 0.76 cm wide slots to allow thermocouple access to the cathode tube surface.

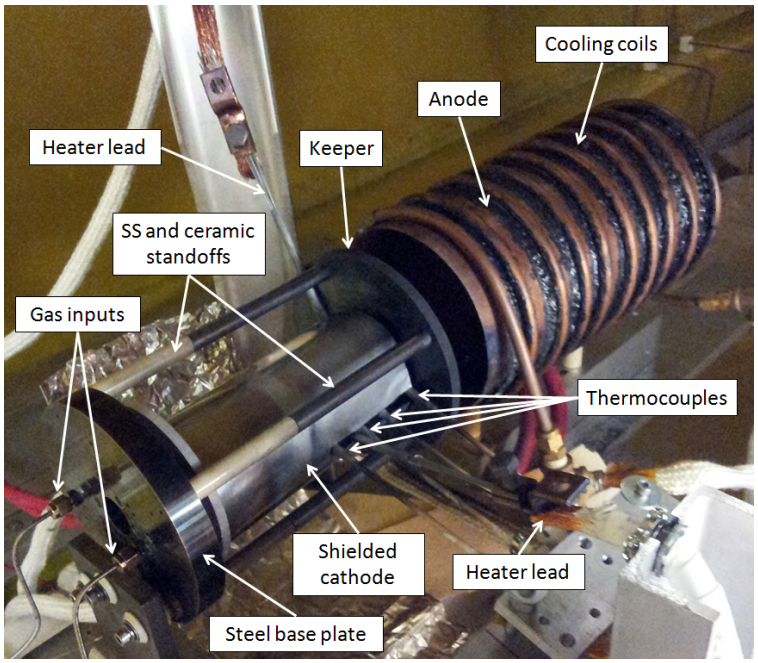

Figure 4. The RF-Controlled Hollow Cathode experiment installed in the tank.

A picture of the experimental setup installed in the tank is shown in Figure 4. We used a 2.5 turn bare tungsten wire for the heater which is wrapped around boron nitride rings for electrical insulation from the cathode. We also added graphite wire beads to stand off the heater wire from the boron nitride insulators, as will be discussed further in Section IV. The heater leads consisted of the heater wire along with many other similar-diameter tungsten wires tightly packed into an alumina tube. This setup allowed for lowering both the electrical resistance and temperature of the leads due a larger effective cross-sectional area. Without the capability to weld tungsten wires together, this heater lead design was a simple way to maintain a high-temperature electrical connection between the tungsten wires that could be disassembled easily. A copper wire lug was used to clamp the tungsten wires of each heater lead to an AWG 00 (2/0) copper welding cable.

Surrounding the heater were three electrically- and thermally-isolated 0.01 cm thick molybdenum sheet heat shields, with slots for thermocouples and heater leads. The graphite keeper plate, 15 cm in diameter and 0.79 cm thick, was placed in front of the cathode. The keeper orifice diameter was 0.96 cm with a 82° chamfer to a final downstream diameter of 2 cm. Four supports held the keeper about 0.13 cm from the downstream graphite edge of the cathode. Each support was a 12 cm long stainless steel rod connected to a 7.6 cm long ceramic stand-off. The steel end of each support was attached to the keeper while the ceramic portion was attached to the cathode baseplate for electrical isolation of the keeper.

The upstream edge of the anode was placed 3.8 cm downstream of the keeper plate. The anode was a 0.08 cm thick copper sheet rolled into a 15 cm diameter, 30 cm long cylinder with ten turns of a 0.95 cm inner diameter water cooling tube wrapped around the outside. A flexible mastic initially provided good thermal contact between the cooling line and the copper sheet. However, at higher anode currents, plasma interactions and anode spot heating rendered parts of the mastic inflexible and the cooling line lost full contact to the cylinder. Due to this reduced thermal contact, recent testing was limited to below 250 A as localized anode melting was witnessed at this high current level. Brazing the water line to the anode cylinder is expected to yield a more robust water-cooled anode capable of much higher currents.

C. Electrical Configuration

As depicted in Figure 5, the experiment was set up in a triode configuration. The heater was connected to an Amrel 32 V, 400 A power supply. The keeper plate was powered by a Sorensen 150 V, 20 A supply. A 50 Ω resistor was placed between the keeper and the Sorensen supply to make it a less attractive pathway for current compared to the anode circuit. The anode was connected to this Sorensen supply and to a Rapid DC 35 V, 650 A supply through diodes; the cathode was grounded. This diode-based electrical circuit allows the keeper power supply's voltage (150 V) to bias both the anode and keeper plate until the lower voltage (35 V) primary anode supply can draw sufficient current to further lower the discharge voltage. At this point the configuration of the diodes causes the keeper to become electrically isolated from the anode. This allows the keeper and anode to be run simultaneously, in parallel, even if their respective power supplies are providing disparate voltages (allowing the anode to bias to the higher of the two supply voltages).

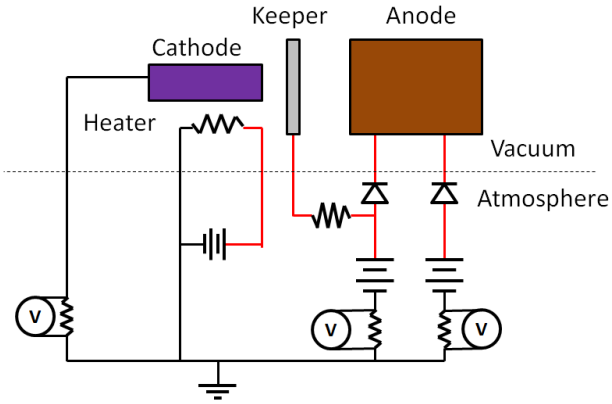

Figure 5. An electrical diagram for the RFC Cathode.

D. Neutral Gas Input

Argon or krypton gas was injected internally through the cathode as seen in Figure 2 and described previously in Section II. The input mass flow was monitored using a variable-area flow meter (also known as a rotometer) capable of processing 0-120 sccm (0-3.6 mg/s) of argon or 0-80 sccm (0-5.0 mg/s) of krypton, where sccm is standard cubic centimeters per minute.

E. Diagnostics

Data for current-voltage traces and axial temperature profiles along the length of the emitter region have been collected to assess the performance of the RFC Cathode. The dependence of these data on neutral gas type as well as the adjustable parameters of mass flow rate and anode discharge current forms the basis of our characterization. For the temperature measurements, the higher heater powers required due to less heat shielding was accepted in exchange for access to the emitter region via thermocouple. We assume that a profile of the temperature along the length of the emitter region can serve as a proxy for current density along the length. Therefore, variation in the current density inside the cathode is shown as variation of the

temperature profile on the cathode surface. Measurement of the cathode temperature profile at different operating points (varying the parameters listed above) allows for a relative comparison of profiles and a qualitative understanding of the trends. We do not expect our measurements of the outside surface of the cathode to match the temperature of the inside surface of the emitter. However, a temperature profile, even of the outside surface, is a relatively straightforward method that could provide evidence of the extent and uniformity of the plasma attachment.

The temperature profile along the length of the emitter region was measured at the outer surface of the graphite tube at four different locations (7.9 cm, 5.4 cm, 3.2 cm and 0.64 cm from the inner surface of the orifice plate) using 36-gauge, tungsten-rhenium C-type thermocouples. These thermocouples were insulated by hafnia which was then coated with molybdenum to an outer diameter of 0.16 cm. These thermocouples were further insulated by a high-temperature zirconia paste and high temperature ceramic tubes (Omega PTRA). This secondary layer of zirconia and ceramic tube was applied as a precaution due to operating in a carbon environment and due to damage observed in one instance, possibly from direct contact with the tungsten heater wire. The temperature of the input and output water of the anode cooling lines was also monitored using two K-type thermocouples to provide another measure of the power flowing to the anode. T-type thermocouples were placed on two vacuum tank windows as the heater can partially radiate to the tank interior, warranting thermal monitoring of these components. All thermocouple readings were independently transmitted wirelessly (via Omega UWTC-1's) to a receiver outside the tank to be recorded by a computer.

Additionally, we measured the temperatures of the tungsten wire heater near the center of the LaB_6 emitter length, the tungsten orifice plate, and the boron nitride microwave window using a disappearing-filament optical pyrometer (Leeds & Northrup Model 8622-C).[22] We calibrated the pyrometer against a cavity blackbody source (Infrared Systems Development Corporation) to establish a maximum calibration error of 4% from the reference temperature. The pyrometer measures radiance at a single wavelength of 650 nm. We made emissivity corrections using the emissivity values at this wavelength for tungsten (0.44 with an estimated error of ± 0.05) and boron nitride (0.31 ± 0.10).[23–25] The transmissivity of acrylic, or poly(methyl methacrylate), at 650 nm[26,27] was also incorporated into the final emissivity correction since the measurements had to be made through acrylic vacuum tank windows. The estimated error of the emissivity values was added to the known error of the pyrometer measurement for the results reported.

Three shunt resistors with an error of 0.01% of the full scale were used to measure the cathode, anode, and keeper currents. Anode, keeper, and heater voltages were measured using voltage dividers connected between those components and ground. Sampling was done at 4 kHz, averaging 2000 samples per data point, with one set of samples being taken each second. These diagnostics were read using a National Instruments DAQ and monitored with LabView.

F. Operational Procedure

After installation in the facility, the system was evacuated to the base pressure of 7×10^{-5} Torr and the heating cycle started. The heater current was gradually increased to 120-130 A over twenty minutes, delivering up to 4 kW of power at maximum current and voltage (132 A, 31.8 V). The neutral gas flow was initiated and set to various values depending on gas species. The cathode supply was set to 35 V while the keeper supply was turned on but limited to zero current. Once the maximum thermocouple temperature reached around 1400 °C, the heater supply was shut off and the keeper voltage was turned up. This cold start procedure[28] prevented arcing and current attachment to the heater. The keeper plasma stabilized with keeper voltages ranging roughly between 25-40 V (at 20 A). Once the discharge had stabilized, the heater was turned on again to aid the transition into high-current operation. This transition took a couple of minutes to occur, after which the discharge current was turned up to at least 100 A to secure a stable plasma. The heater was then turned off as the fully established discharge was self-sustaining at voltages below the anode supply limit. The anode current limit could then be set at the desired operating condition until steady state was reached.

IV. Experimental Results and Discussion

A. Ignition and Operation

Following the operational procedure described in Section III, the steady-state pre-ignition temperature profile shown in Fig. 6 was obtained repeatedly (±30 C, 95% confidence). The locations of the temperature measurements are given in Fig. 7. Figure 8 shows the voltages required to start the cathode discharge (applied using the keeper supply) for a range of argon and krypton flow rates. It is relevant for future large-cathode design and operation to note that much higher argon flow rates were required to achieve similar ignition voltages than those obtained using krypton (up to 80 sccm more for argon at the same ignition voltage, or up to a 40 V difference for comparable flow rates).

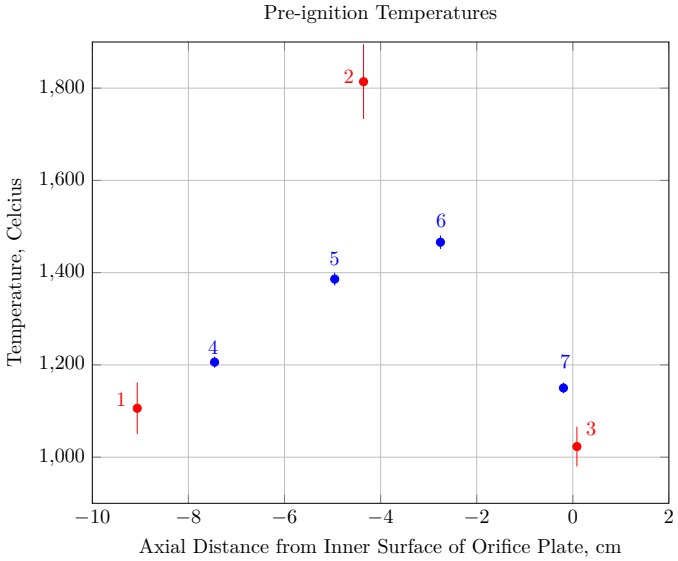

Figure 6. Temperature measurements taken prior to plasma ignition as a function of the distance from the inner surface of the orifice plate along the cathode major axis. 1-3 in red are pyrometer measurements (1 is the microwave window, 2 is the heater wire, and 3 is the orifice plate) and 4-7 in blue are thermocouple measurements of the outer cathode surface.

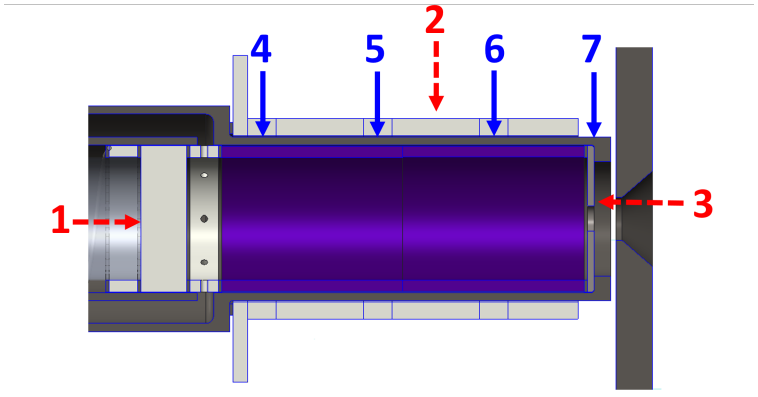

Figure 7. Locations of temperature measurements. 1-3 in red are pyrometer measurement locations (1 is the window, 2 is the heater wire, and 3 is the orifice plate) and 4-7 in blue are thermocouple measurements of the outer graphite surface of the cathode emitter region. (Slots exist in the boron nitride insulators for the thermocouples to touch the cathode wall directly.)

For low-current operation at approximately 20 A of anode current, we found that the steady-state voltages (Fig. 9) and cathode temperatures (Fig. 10) tended to decrease with increasing flow rate, and shifted

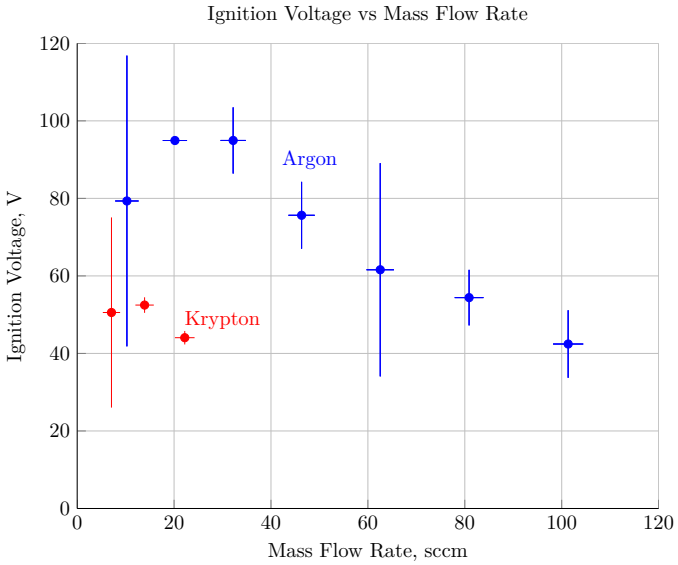

Figure 8. Discharge initiation voltage as a function of internal mass flow rate in sccm for selected operating points using argon and krypton gas.

substantially with changes in the gas type. All of the measured thermocouple temperatures along the cathode body showed a decreasing trend with increasing flow rate, in contrast to the trend in orifice plate behavior reported in Ref. 29.

The RFC Cathode was able to reach stable operation at a range of argon and krypton flow rates at a current of approximately 20 A. This current is comparable to the minimum self-heating condition presented for Goebel's 2 cm LaB_6 hollow cathode,[6] although the discharge voltage is much higher (likely due to differences in thermal insulation and gas species). We found that initiating a discharge between the cathode and keeper, and even extracting small currents to the anode ($\approx$ 20 A) could be effected with relative ease; causing the anode to pull larger currents proved to be more difficult for the gases and power supplies used. In order to transition to high-current operation, the full keeper supply current (split predominantly toward the anode) was maintained and the heater was reactivated up to 4 kW in order to reduce the discharge voltage to below 35 V (the voltage limit for our high-current anode supply). For the tested configuration, we could only meet this power-supply-induced restriction using krypton. We have drawn anode currents up to 250 A with krypton, and expect to be able to draw much higher currents (e.g. 400 A) with an improved water-cooled anode.

Steady-state operation was achieved for anode currents between 20 and 225 A using krypton, though for currents below 30 A the discharge voltage surpassed the limit of our high-current supply. The voltage behavior of the RFC Cathode as a function of current for a fixed flow rate of 42 ($\pm$2) sccm krypton and a fixed keeper current of 2.2 A is shown in Fig. 11. The minimum or dip in the anode voltage and the essentially monotonic decrease in keeper voltage as anode current is increased are expected qualitative behaviors and have been observed in the literature.[2,6]

The steady-state thermocouple temperatures as a function of discharge current at the previously mentioned operating condition with krypton are shown in Fig. 12. It is noteworthy that while the RFC Cathode operates at higher discharge voltages than those for prior cathodes,[2,6] it appears to operate at lower temperatures, especially near the orifice. Goebel's 2 cm cathode operates at temperatures between 1500 and 2200°C at the orifice plate, whereas the closest thermocouple to the cathode orifice plate in our configuration never exceeded 800°C for the currents tested. It is important to note that this thermocouple measurement is not a direct measure of the orifice temperature, but still provides information regarding the maximum orifice temperature. Rather than at the closest location to the orifice, the maximum thermocouple temperature occurred at the next upstream measurement location (thermocouple #6 in Fig. 12). The variation in temperature along the cathode tube length is much larger than the 5% variation in emitter temperature along the emitter length reported for prior large cathodes.[6] The variation in temperature along the cathode tube and the location of the maximum temperature are consistent across the tested discharge currents, though

the thermocouple measurements of the cathode tube are not necessarily representative of the emitter temperatures or their variation along the cathode length. These observations suggest that the RFC Cathode operates at lower, but less-uniform, temperatures than comparably sized laboratory LaB_6 cathodes at the same currents. More direct measurements will be needed to determine if these temperature variations are consistent between the cathode tube and emitter itself.

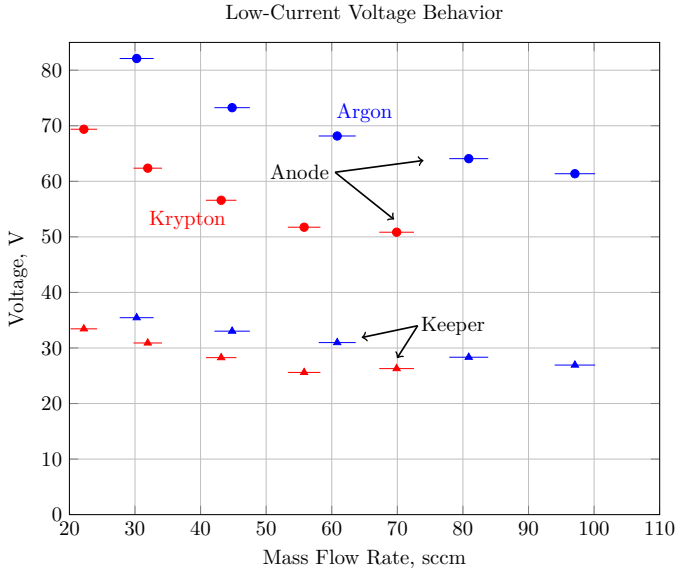

Figure 9. A comparison of the anode and keeper voltages versus mass flow rate for argon and krypton at approximately 20 A anode current.

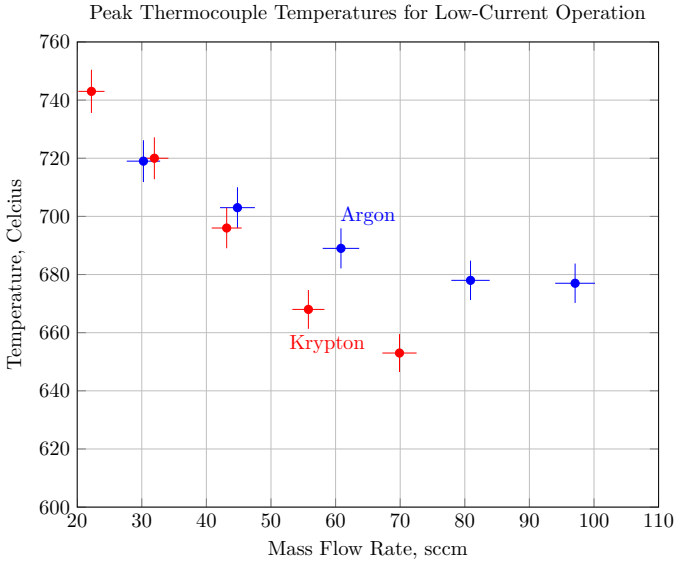

Figure 10. A comparison of peak thermocouple measurements versus mass flow rates of krypton and argon. The mass flow rates for each gas are offset from each other due to different flow meter corrections for each gas.

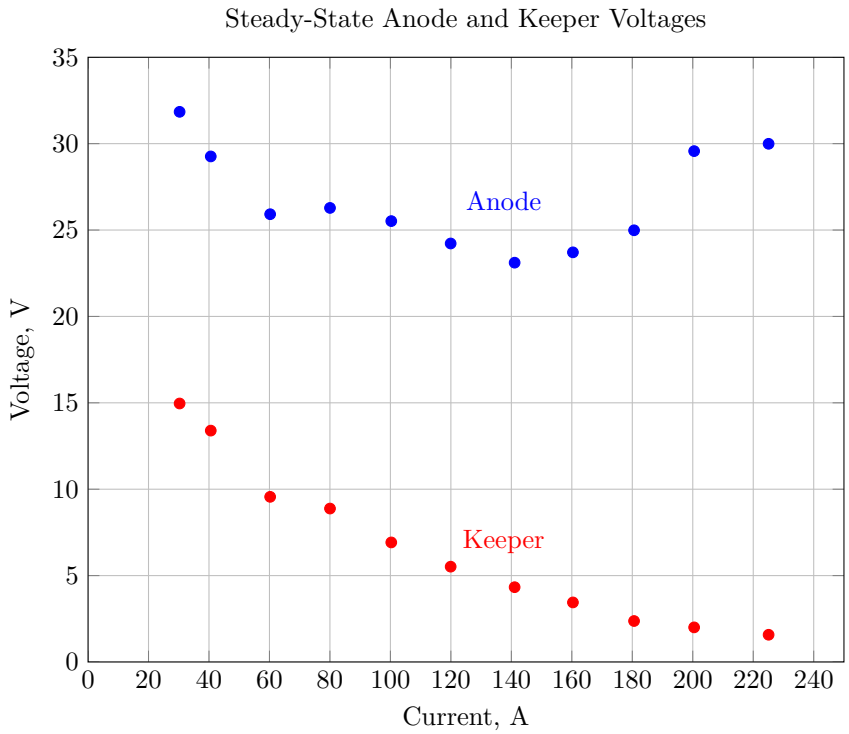

Figure 11. Anode and keeper voltages versus anode current for operation with krypton. The keeper current was held constant at 2.2 A and the mass flow rate was fixed at 42 sccm. The measurement error bars are smaller than the plot markers used.

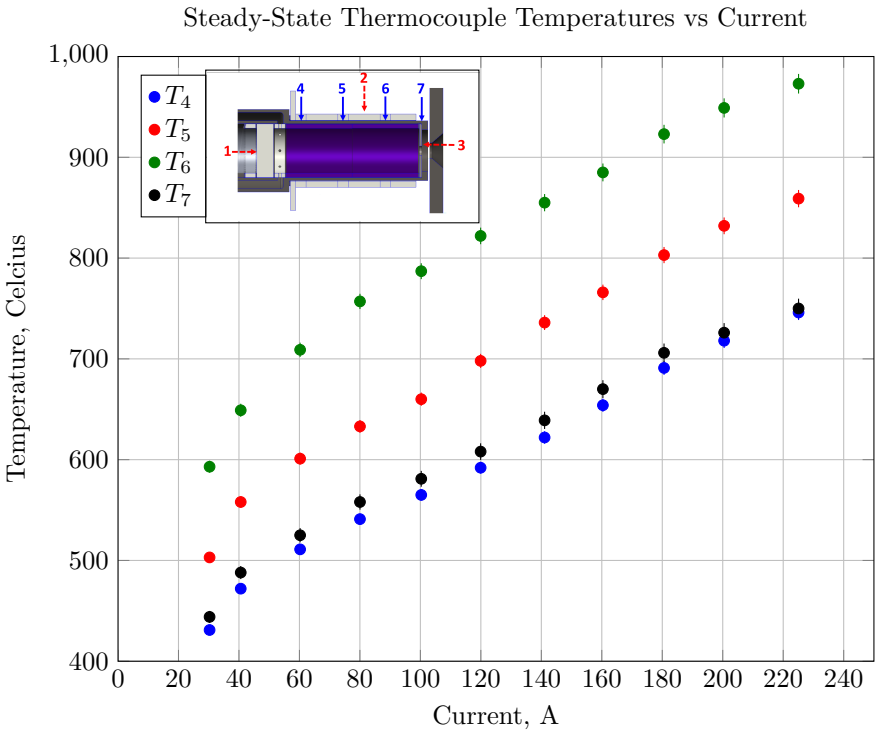

Figure 12. Thermocouple temperatures vs discharge current at a constant mass flow rate of 42 sccm and 2.2 A keeper current.

B. Heater Failure Modes

We have experienced multiple heater failures while experimenting. Failures are often presaged by degradation in the heater as evidenced by an increase of the heater circuit resistance. While multiple factors seen in the literature like thermal gradients, nonuniform vaporization, and hot spots inherent to tungsten filaments can cause them to fail,[30] these failures generally occur over longer timescales (hundreds of hours or more) than those observed during this experiment. At worst, we have had a heater fail in less than two brief, but high-temperature, thermal cycles. Since there are no significant mechanical loads on the wire, the likely short term causes of failure are arcing or material interactions. We expect that one of these causes is dominant for all of our failure cases.

Arcing failures of the heater can be correlated to witnessing events during experimentation, usually resulting in failure soon after. Post-run inspection of the wire reveals clear melting at the break joint. The prevalence of arcing failures was exacerbated by exploration of the operational envelope and the ignition procedure. However, after tweaking the design and learning the appropriate parameters for igniting and operating the RFC Cathode, we have not had significant arcing problems. Arcing would be solved robustly if a suitable insulating ceramic and fabrication process were found that could completely isolate the heater wire and withstand temperatures approaching 2000°C.

The second short-term cause of heater failure we have witnessed is material interaction. As seen in Fig. 13, visible damage is incurred by the tungsten wire and boron nitride insulating rings during operation. This damage only occurs where the tungsten and boron nitride are in contact and furthermore, wire breaks of this nature only occur along these damaged areas of contact. To explain the source mechanism behind this failure, the literature explains that bulk tungsten and boron nitride can start to interact chemically to produce various tungsten borides when in contact and at temperatures starting between 800 and 1200°C.[31–34] The quantity of the various tungsten borides created increases with both time and temperature. From Ref. 31 we calculated the expected cross-sectional area of boron diffusion to be greater than 7% of our original tungsten wire cross-section when operated at 1400°C for 30 minutes. Pyrometer measurements of our bare tungsten heater wire in Fig. 6 show that the heater is often at much higher temperatures than this, and at our operational extreme, the heater temperature has peaked at over 1800°C.

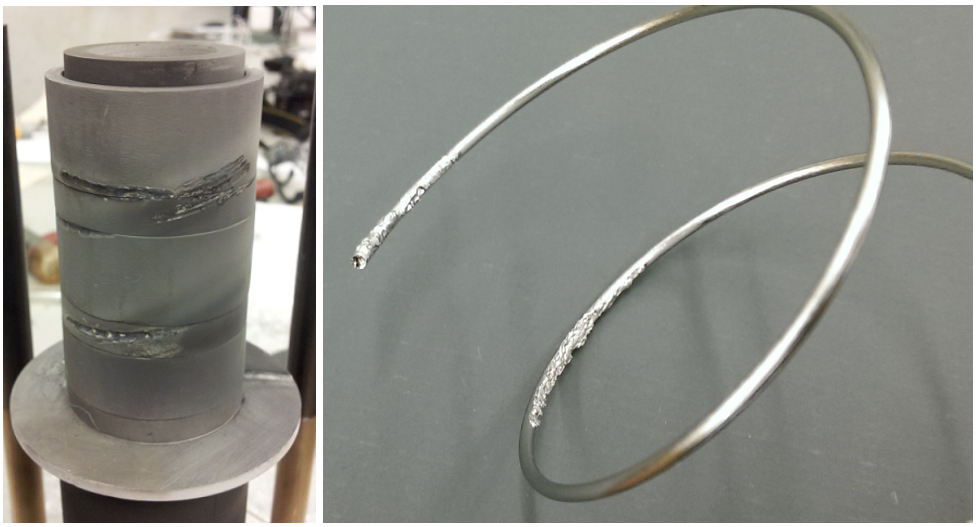

Figure 13. Pictured are examples of damaged boron nitride rings (left) and broken tungsten heater wire (right).

Tungsten borides are more resistive and have a different thermal expansion coefficient than tungsten[31,35–37] and are known to be brittle.[31,32] The mechanism by which we expect these heater failures occur starts with the formation of tungsten borides on the tungsten heater. The tungsten borides' higher resistivity than tungsten locally increases the temperature at a given heater current. This local heating aggravates cracking due to the difference in thermal expansion between the tungsten substrate and surface tungsten borides. The embrittled region experiences strong temperature gradients and increasing stress from differential thermal expansion until failure occurs. This is the suspected physical mechanism by which failure in this type of

large-diameter cathode heater occurs.

As a possible solution, we are testing graphite wire beads to separate the tungsten from the boron nitride. We assume most of the heat transfer is accomplished through radiation since the heater wire is typically in little direct contact with the insulating rings. Carbon beads do not seem to significantly change the thermal contact in our case. The carbon and tungsten could interact but carburization is usually slow and incomplete in a vacuum or argon environment. Tungsten carbide is not as brittle as tungsten borides and so we do not expect their potential creation at the surface to lead to a similar failure as demonstrated with tungsten borides.[37]

V. Conclusion

The purpose of this paper was to illuminate the design and operational challenges of large-diameter hollow cathodes. We found that bare, high-temperature tungsten wire heaters can fail often due to arcing and undesirable material interactions. A proposed solution, carbon wire beads, has been presented and is under testing. As our research on high-temperature heaters is exploratory, we expect that there is significant progress yet to be made in this area for large-scale thermionic hollow cathodes.

We have found that the RFC Cathode operates in a self-heating mode at a very similar minimum current ($\approx$ 20 A) to prior large cathodes, despite large differences in scale. While a direct comparison of the discharge voltages for given output currents of other laboratory cathodes provides limited insight due to thermal and gas species differences, the voltage behavior of the cathode follows previously observed trends with increasing discharge current. The thermal behavior of the RFC Cathode, however, displays temperature variation with increasing mass flow that opposes previously reported trends in orifice temperature,[29] though further investigation of the effect of mass flow on discharge voltage as a function of discharge current is needed to further characterize this behavior. Planned future work involves the further characterization of the behavior of the large-diameter RFC Cathode, along with the determination of the effects of the addition of varying RF power.

Acknowledgments

We thank the U.S. Air Force Office of Scientific Research for supporting this research. We also thank Bob Sorenson for his assistance and expertise in the fabrication of this experiment.

References

[1]Brown, D. L., Beal, B. E., and Haas, J. M., "Air Force Research Laboratory High Power Electric Propulsion Technology Development," IEEEAC, 2009.

[2]Goebel, D. M. and Chu, E., "High Current Lanthanum Hexaboride Hollow Cathodes for High Power Hall Thrusters," 32nd International Electric Propulsion Conference, Jet Propulsion Laboratory, Wiesbaden, Germany, 2011, pp. 1–16.

[3]Soulas, G. C., Haag, T. W., Herman, D. A., Huang, W., Kamhawi, H., and Shastry, R., "Performance Test Results of the NASA-457M v2 Hall Thruster," 48th AIAA Joint Propulsion Conference, Atlanta, Georgia, 2012, pp. 1–17.

[4]Hofer, R. R., Randolph, T. M., Oh, D. Y., Snyder, J. S., and de Grys, K. H., "Evaluation of a 4.5 kW Commercial Hall Thruster System for NASA Science Missions," 42nd Joint Propulsion Conference, Sacramento, California, 2006.

[5]Goebel, D. M. and Chu, E., "High Current Lanthanum Hexaboride Hollow Cathode for 20-to-100 kW Class Hall Thrusters," 48th AIAA Joint Propulsion Conference, Atlanta, Georgia, 2012, pp. 1–11.

[6]Goebel, D. M. and Chu, E., "High-Current Lanthanum Hexaboride Hollow Cathode for High-Power Hall Thrusters," Journal of Propulsion and Power, Vol. 30, No. 1, Jan. 2014, pp. 35–40.

[7]Van Noord, J. L., Kamhawi, H., and Mcewen, H. K., "Characterization of a High Current, Long Life Hollow Cathode," IEPC, No. February, Princeton, New Jersey, 2005, pp. 1–12.

[8]Diamant, K. D., "Resonant Cavity Plasma Electron Source," IEEE Transactions on Plasma Science, Vol. 37, No. 8, Aug. 2009, pp. 1558–1562.

[9]Foster, J. E. and Patterson, M. J., "Characterization of 40-Centimeter Microwave Electron Cyclotron Resonance Ion Source and Neutralizer," Journal of Propulsion and Power, Vol. 21, No. 5, 2005, pp. 1–5.

[10]Katz, I., Mikellides, I. G., Goebel, D. M., and Polk, J. E., "Insert Heating and Ignition in Inert-Gas Hollow Cathodes," IEEE Transactions on Plasma Science, Vol. 36, No. 5, 2008, pp. 2199–2206.

[11]Goebel, D. M. and Katz, I., Fundamentals of Electric Propulsion: Ion and Hall Thrusters, Vol. 1, John Wiley & Sons Inc, 2008.

[12]Polk, J. E., Mikellides, I. G., Katz, I., and Capece, A. M., "Tungsten and Barium Transport in the Internal Plasma of Hollow Cathodes," Journal of Applied Physics, Vol. 105, No. 11, 2009, pp. 113301.

[13]Goebel, D. M., Jameson, K. K., and Hofer, R. R., "Hall Thruster Cathode Flow Impact on Coupling Voltage and Cathode Life," Journal of Propulsion and Power, Vol. 28, No. 2, March 2012, pp. 355–363.

[14]Goebel, D. M., Watkins, R. M., and Jameson, K. K., "LaB6 Hollow Cathodes for Ion and Hall Thrusters," Journal of Propulsion and Power, Vol. 23, No. 3, May 2007, pp. 552–558.

[15]Plasek, M. L., Wordingham, C. J., Choueiri, E. Y., and Polk, J. E., "Modeling and Development of the RF-Controlled Hollow Cathode Concept," 49th Joint Propulsion Conference, San Jose, CA, 2013, pp. 1–3.

[16]Plasek, M. L., Wordingham, C. J., and Choueiri, E. Y., "Resonant Mode Transition in the RF-Controlled Hollow Cathode," 33rd International Electric Propulsion Conference, Washington, D.C., 2013.

[17]Salhi, A. and Turchi, P. J., "Scaling Relations for Design and Operation of Orificed-Hollow Cathodes," 30th Joint Propulsion Conference, Indianapolis, Indiana, 1994, pp. 0–7.

[18]Goebel, D. M., Jameson, K. K., Katz, I., and Mikellides, I. G., "Plasma Potential Behavior and Plume Mode Transitions in Hollow Cathode Discharges," 30th International Electric Propulsion Conference, Vol. 14, Florence, Italy, 2007, p. 103508.

[19]Goebel, D. M. and Watkins, R. M., "Compact Lanthanum Hexaboride Hollow Cathode," Review of Scientific Instruments, Vol. 81, No. 8, Aug. 2010, pp. 083504.

[20]Chu, E., Goebel, D. M., and Wirz, R. E., "Reduction of Energetic Ion Production in Hollow Cathodes by External Gas Injection," Journal of Propulsion and Power, June 2013, pp. 1–9.

[21]Tighe, W., Freick, K., and Chien, K., "Performance evaluation and life test of the XIPS hollow cathode heater," JPC, No. AIAA 2005-4066, 2005, pp. 1–11.

[22]Motzfeldt, K., High Temperature Experiments in Chemistry and Materials Science, John Wiley and Sons, 2012.

[23]MuÌĹller, B. and Renz, U., "Development of a fast fiber-optic two-color pyrometer for the temperature measurement of surfaces with varying emissivities," Review of Scientific Instruments, Vol. 72, No. 8, 2001, pp. 3366.

[24]Svet, D., Thermal radiation: metals, semiconductors, ceramics, partly transparent bodies, and films, New York, 1965.

[25]Sala, A., Radiant Properties of Materials: Tables of Radiant Values for Black Body and Real Materials, Elsevier Science Ltd, 1986.

[26]Gooch, J. W., Encyclopedic Dictionary of Polymers, Springer New York, 2nd ed., 2011.

[27]Joram, C., "Transmission curves of plexiglass (PMMA) and optical grease," Tech. Rep. October, CERN, PH-EP, 2009.

[28]Vaughn, J., "Life Testing of the Hollow Cathode Plasma Contactor for the ProSEDS Mission," Spacecraft Charging . . . , 2001, pp. 2–7.

[29]Kamhawi, H. and Van Noord, J., "Development and Testing of High Current Hollow Cathodes for High Power Hall Thrusters," 48th AIAA Joint Propulsion Conference, Atlanta, Georgia, 2012, pp. 1–13.

[30]Horacsek, O., "Properties and failure modes of incandescent tungsten filaments," IEE Proceedings A, Vol. 127, No. 3, 1980.

[31]Usta, M., Ozbek, I., Ipek, M., Bindal, C., and a.H. Ucisik, "The characterization of borided pure tungsten," Surface and Coatings Technology, Vol. 194, No. 2-3, May 2005, pp. 330–334.

[32]Khor, K., Yu, L., and Sundararajan, G., "Formation of hard tungsten boride layer by spark plasma sintering boriding," Thin Solid Films, Vol. 478, No. 1-2, May 2005, pp. 232–237.

[33]Rogl, P., "Materials science of ternary metal boron nitrides," International Journal of Inorganic Materials, Vol. 3, No. 3, June 2001, pp. 201–209.

[34]Itoh, H., Matsudaira, T., and Naka, S., "Formation process of tungsten borides by solid state reaction between tungsten and amorphous boron," Journal of materials . . . , Vol. 22, 1987, pp. 2811–2815.

[35]Wang, C., Akbar, S., Chen, W., and Patton, V., "Electrical properties of high-temperature oxides, borides, carbides, and nitrides," Journal of materials science, Vol. 30, 1995, pp. 1627–1641.

[36]Juretschke, H. and Steinitz, R., "Hall effect and electrical conductivity of transition-metal diborides," Journal of Physics and Chemistry of Solids, Vol. 4, 1958, pp. 118–127.

[37]Lassner, E. and Schubert, W., Tungsten, Springer Science, 1999.